# Drained Triaxial Tests in Low-Permeability Shales: Application to the Callovo-Oxfordian Claystone

Malik Belmokhtar, Pierre Delage, Siavash Ghabezloo, Nathalie Conil

# Drained triaxial tests in low permeability shales. Application to the Callovo-Oxfordian claystone

*Malik Belmokhtar[1], Pierre Delage[1], Siavash Ghabezloo[1], Nathalie Conil[2]*

*[1] Ecole des Ponts ParisTech, Laboratoire Navier/CERMES, 6-8 av. B. Pascal, F77455 Marne la Vallée, France.*

*[2]Andra, Bure, France.*

***Abstract***

*Drained triaxial testing is challenging in low permeability claystones ($10^{-20}$ $m^2$). This paper presents a method of testing low permeability clay rocks in a standard triaxial cell. In this system, the resaturation of the specimen and the drainage conditions were enhanced by reducing the drainage length to 19 mm, the specimen radius. To do so, two geotextiles were placed around the top and bottom ends of the specimen, with no connection between them. Resaturation was hence performed by forcing water infiltration into the specimen from the upper and lower geotextiles, with a maximum infiltration length of around 19 mm, resulting in reasonable saturation durations. High precision local measurements of radial strains were also achieved by ensuring direct contact between the LVDT rod and the specimen through the membrane. A poroelastic numerical calculation was carried out, and it was shown that, with these drainage conditions, a strain rate of $6.6\times10^{-8}$ $s^{-1}$ was satisfactory to ensure good drainage when shearing claystone specimens. After a check test made on a low permeability sandstone with well-known mechanical characteristics, two tests were carried out to investigate specimens of the Callovo-Oxfordian claystone, a possible host rock for deep geological disposal in France. The results compare well with other published data from drained triaxial tests.*

**Keywords:** Triaxial testing, low permeability, claystone, shale, drainage length, strain rate, poroelasticity.

## 1. Introduction

Geological deep formations are considered as possible natural barriers and host formations in the framework of multi-barriers concepts used for long term disposal of high level radioactive wastes. Some European countries selected low permeability and low porosity rocks, according to the geology of the country. In Sweden (in the Aspo Hard Rock Laboratory - HRL) and Switzerland (in the Grimsel Underground research laboratory - URL) diorite and granite formations are considered, respectively, whereas claystones and clays are considered in France, Switzerland and Belgium. In France, the mechanical behaviour of the Callovo-Oxfordian (COx) claystone is investigated in the Bure URL by Andra, the French Agency for the management of radioactive wastes. In Switzerland, the mechanical behaviour of the Opalinus Clay is investigated in the Mont Terri Rock Laboratory managed by SWISSTOPO (Swiss Federal Office of Topography), in collaboration with Nagra (the Swiss Agency for the management of radioactive wastes). In Belgium, the Boom clay is investigated in the Mol URL by the Euridice research organisation.

Besides radioactive waste disposal issues, the investigation of the mechanical behaviour of claystone and shales has also been conducted for various other purposes, including borehole stability for conventional oil and gas production (e.g. *Steiger and Leung 1991*, *Schmitt et al. 1994*, *Aoki 1995*, *Islam and Skalle 2013*), the production of shale oil and gas (e.g. *Ewy et al. 2003, Eseme et al. 2007, Villamor-Lora et al. 2016*), tunnelling issues (e.g. *Einstein 2000, Bonini et al. 2009*), and $CO_2$ sequestration (*Busch et al. 2008*).

The very low permeability of clays and claystones (in the order of $10^{-19}$ m$^2$ for clays and $10^{-20}$ m$^2$ for claystones) is an essential feature for the safe confinement of radioactive wastes. However, low permeability results in significant difficulties in the hydro-mechanical testing of claystones. Indeed, fully drained triaxial testing with standard triaxial claystone specimens (height of 76 mm and diameter of 38 mm) requires quite slow loading rates that result in long testing periods. By solving Terzaghi's equation of consolidation, *Gibson and Henkel (1954)* determined appropriate axial strain rates for drained triaxial testing of fine grained soils specimens (see also Wissa 1969). As stated in *Bishop and Henkel (1957)*, it is currently accepted that a value of 1μm/mn ($2 \times 10^{-7}$ s$^{-1}$) is appropriate to carry out drained tests on standard triaxial specimens in soils. Chiu et al. (1983) extended these concepts to drained triaxial testing on a Melbourne mudstone. Recalling that the combined effects of sampling, storage, preparation and mounting almost certainly caused some loss of moisture in mudstones that are saturated in-situ, they carefully re-saturated the specimens prior to triaxial testing. They

found that a strain rate of $3.3 \times 10^{-7}$ s$^{-1}$ was appropriate to ensure satisfactory dissipation of excess pore pressure during the test. Note however that, with 70% silt sized and 28% clay sized particles, and a porosity around 25%, the Melbourne mudstone is probably more permeable than the claystones considered here, that are denser (porosity between 13 and 17%) and have more than 50% clay fraction. Following *Chiu et al. (1983)*, *Swan et al. (1989)* examined in detail the strain rate effects in Kimmeridge Bay shale, a shale with a mean permeability of $8 \times 10^{-21}$ m$^2$ under 10 MPa. They performed some poroelastic finite elements calculations of pore pressure generated during triaxial testing and showed that, with a specimen of 50 mm height and 25 mm in diameter with lateral drainage (drainage length 12.5 mm), an axial strain rate of $8.3 \times 10^{-7}$ s$^{-1}$ was low enough to avoid any pore pressure generation during shear. *Wu et al. (1997)* investigated the behaviour of the Pierre II shale by using the same specimen size as *Swan et al. (1989)*, with lateral drainage made by fibreglass sidedrains placed around the specimen. They observed that a rate of $3 \times 10^{-8}$ s$^{-1}$ was sufficient to ensure homogeneous pore pressure within the specimens during undrained loading. In the same context, *Islam and Skalle (2013)* performed a series of triaxial tests with standard triaxial specimens of Pierre I shale with strain rates of 1-2 $\times 10^{-7}$ s$^{-1}$ for undrained tests and $2 \times 10^{-8}$ s$^{-1}$ for drained tests.

As stated by *Chiu et al. (1983)*, claystone and shale specimens may be partially saturated before testing, due to the successive processes of coring, transport, conservation and trimming in the laboratory (see also *Monfared et al., 2011a; Ewy, 2015*). They hence have to be re-saturated prior to testing, a process that can be long in low permeability claystones. Resaturation is not too difficult in non-swelling mudstone like that tested by *Chiu et al. (1983)*, who put the specimens of Melbourne mudstone under vacuum, prior to completely immersing them in de-aired water in a desiccator. Things are more complicated in swelling claystones like the COx claystone, the Opalinus Clay and the Tournemire shale, with significant swelling occurring when putting the specimens in contact with water (*Schmitt et al. 1994*).

Swelling claystones are quite sensitive to changes in water content, as observed by *Chiarelli et al. (2003), Valès et al. (2004), Zhang and Rothfuchs (2004), Pham et al. (2007) and Zhang et al. (2012).* As mentioned by *Menaceur et al. (2015)*, besides drainage issues, the differences in testing procedures with respect to the partially saturated states of the specimens are one of the reasons, beside natural variability, of the differences observed in the shear strength properties of claystones. Partial saturation and poor drainage may lead to biased assessment of the mechanical properties of the tested specimens, over-estimating the shear strength with partially saturated specimens, and over-estimating the Young's modulus by

running partially drained tests. Furthermore, the long duration of the resaturation process in standard triaxial tests drained on top and bottom with a drainage length of 38 mm (mid-height of standard triaxial specimen) makes it difficult to carry out fully drained tests in properly saturated specimens within a reasonable period of time.

In this regard, the hollow cylindrical triaxial apparatus (hollow cylinder specimens of 100 mm external diameter, 60 mm internal diameter and 70 mm height, with drainage ensured on both the inner and outer faces) developed by *Monfared et al. (2011)* reduced the drainage length down to half the thickness of the hollow cylinder, say 10 mm. *Hu et al. (2014)* adopted small-sized triaxial specimens (20 mm in height and diameter) drained on top and bottom, resulting in a drainage length of 10 mm as well (half the height of the specimen). This small drainage length, four times smaller than standard triaxial drainage length (38 mm), reduces the pore pressure diffusion rate by a factor of 16 compared to standard triaxial specimens (*Monfared et al., 2011*). As shown by *Monfared et al. (2011), Mohajerani et al. (2013), Menaceur et al. (2015) and Menaceur et al. (2016a)* with hollow cylinder specimen and by *Hu et al. (2014)* with small-sized specimen, the 10 mm drainage length made it possible to achieve satisfactory saturation within 3 to 4 days, compared to a period of around one month in standard triaxial tests. Reasonable results of fully saturated and drained isotropic compression tests have also been obtained for the COx claystone with a 10 mm high specimen drained at the bottom, also resulting in a 10 mm drainage length (*Mohajerani et al. 2012; Belmokhtar et al. 2017a, 2017b*). Based on satisfactorily drained tests, *Belmokhtar et al. (2017a)* determined a set of transverse isotropic poroelastic parameters of the COx claystone.

In this study, a high precision triaxial testing system with enhanced drainage aimed at testing standard triaxial specimens of low permeability clay rocks (38 mm in diameter and 76 mm in height) is presented. Poroelastic calculations are carried out to determine the relevant axial strain rate allowing satisfactory drainage, and the system is used to determine the shear strength properties of the COx claystone.

## 2. Material and methods

*The Callovo-Oxfordian claystone*

The specimens of the Callovo-Oxfordian claystone tested (core EST51338) were extracted at a depth of 490 m at the level of the Andra Underground Research Laboratory, located in Northeast of France near the village of Bure (Figure 1). The COx claystone is a 155 million years old sedimentary rock, with a layer thickness of about 150 m, covered by an

Oxfordian limestone layer and deposited upon a Dogger limestone layer. At the depth of extraction, the COx is composed mostly of clays (45-50%, with 10-24% interstratified illite/smectite layers, 17-21% illite, 2-3% chlorite) and contains also 28% carbonate, 23% quartz and 4% of other minerals (Gaucher et al., 2004). The mixed layer illite-smectite fraction in the clay matrix produces some swelling properties (e.g. *Mohajerani et al., 2012; Delage et al., 2014*) and interesting self-sealing capabilities (e.g. *Davy et al., 2007; Zhang, 2011; Menaceur et al. 2015*). The clay and carbonate contents of the COx claystone vary with depth, with total porosity between 14% in carbonated levels and 19.5% in the most argillaceous levels (*Yven et al., 2007*) in which the URL has been excavated.

The in-situ state of stress in the Bure URL has been investigated in detail by *Wileveau et al. (2007)*, who estimated a vertical lithostatic total stress $\sigma_v$ = 12.7 MPa , a major horizontal stress $\sigma_H$ = 14.8-16 MPa, a minor horizontal stress $\sigma_h$ = 12.4 MPa and a hydrostatic pore pressure $p_w$ = 4.9 MPa. Typical characteristics of the COx claystone are a very low permeability (in order of $10^{-20}$ $m^2$, *Escoffier, 2002; Davy et al., 2007; Zhang, 2011; Menaceur et al., 2015, 2016)*, a good ability to retain radionuclides and a low diffusion coefficient, resulting in very slow solute transfer.

The two specimens tested in this study (EST51338a and b) come from a 80 mm diameter core oriented perpendicularly to the horizontal bedding plane of the COx claystone layer at Bure (see Figure 1). They were trimmed from the core by using a diamond core of 38 mm diameter, prior to cutting them to the required length (around 76 mm) by using a diamond saw. The water content was determined on two slices cut on the top and bottom of the specimen by oven drying at 105°C during 48 hours. The specimen volume was determined by hydrostatic weighing to calculate the total porosity and the initial degree of saturation.

The initial characteristics of the specimen are presented in Table 1. The water content was 5.97%, corresponding to a degree of saturation of 87.9%, considering a particle density $\rho_s$ = 2.70 $Mg/m^3$ (Andra, 2005). A suction measurement was carried out on some the cuttings of the specimen by using a chilled mirror tensiometer (WP4C, Decagon), providing a value of 36.2 MPa, in good agreement with the water retention curves provided by *Pham et al. (2007) and Wan et al. (2013)*. These data indicate a slight desaturation of the specimen.

*Experimental set-up*

A schematic view of the device is shown in Figure 2, together with a photo showing the specimen wrapped into the upper and lower geotextiles. The device consists of a conventional

high pressure triaxial cell, hosting a standard triaxial specimen (38 mm in diameter and 76 mm in height), and connected to three pressure volume controllers (PVC, GDS Brand). The confining pressure is applied in the cell through a confining fluid (silicone oil) that is put under pressure by a PVC (maximum value 64 MPa), whereas 2 other PVCs independently apply the back pressure through the porous disks placed on the top and bottom of the specimen, respectively. The pore pressure can be measured by two pressure transducers (PT) connected to the top and bottom of the specimen, respectively.

As also presented in Figure 2, enhanced drainage conditions are ensured by placing two bands of geotextile on the upper and lower parts of the specimen, with no contact between them. Both geotextiles are in contact with the corresponding porous stones. The drainage length is hence reduced to the specimen radius, i.e. 19 mm. The drainage performances of *the* geotextile under pressure had been checked by *Monfared (2011)*.

At mid-height of the specimen, a layer of around 1 cm was left without any geotextile in contact so as to avoid any connection and water exchange between the upper and lower geotextiles. Saturation is then possible by forcing the infiltration of water into the specimen from both geotextiles on top and bottom, allowing specimen resaturation within a short enough period of time, thanks to the 19 mm maximum infiltration length (if connected, the geotextiles would have worked as a by-pass between the top and bottom porous stones). This arrangement also produced direct contact between the specimen and the stems of the four radial LVDTs used for the local measurement of radial strain. Direct contact was ensured by piercing the (neoprene) membrane with a hole smaller in diameter than the stem. Fluid tightness was ensured by putting a drop of neoprene glue on the membrane around the stem. The confining fluid used was a silicone oil. The effectiveness of the direct contact between the LVDT and the specimen has been demonstrated in *Belmokhtar et al. (2017a)* and a precision of ±0.1 μm corresponding to a strain of $10^{-5}$ was obtained. Two axial LVDTs were supported by a system of rings as shown in Figure 2b, following the system adopted in *Monfared et al. (2011)*.

Figure 3 shows a specimen a specimen mounted with the system supporting the four radial and two axial LVDTs. The shear strain rate was controlled by using a loading frame with a capacity of 25 tons. The axial force was directly measured by an immersed force sensor with a maximum capacity of 25 kN. The cell temperature was controlled at 25°C ± 0.1°C by a resistive electric heating belt placed around the cell. The specimen temperature was measured by a thermocouple placed close to the specimen inside the stainless-steel confining cell. Thermal isolation was improved by covering the cell with an insulating layer.

*Drained shear rate*

Together with the drainage length, the value of the strain rate adopted in triaxial shear tests is of crucial importance with respect to the quality of drainage. Typically, in fine-grained soils, a displacement rate of 1 μm/min (strain rate of $2.2\times10^{-7}$ $s^{-1}$) is adopted in standard triaxial specimens (78mm height and 38 mm diameter, permeability $k$ around $10^{-18}$ $m^2$). The drainage length is reduced to 19 mm (specimen radius) by placing filter papers all around the vertical faces of the specimen. Filter papers are connected to specimen ends to accelerate consolidation and pore pressure dissipation (*Gibson and Henkel 1954; Bishop and Henkel 1957*). Based on soil mechanics procedures, *Wu et al. (1997)* adopted a strain rate of $3\times10^{-8}$ $s^{-1}$ on a laterally drained 50 mm long specimen of low permeability Pierre II shale to ensure pore pressure homogeneity in an undrained test. The drainage length was $h$ = 12.5 mm. Similarly, *Islam and Skalle (2013)* adopted rates of 1-$2\times10^{-7}$ $s^{-1}$ in undrained tests and $2\times10^{-8}$ $s^{-1}$ in drained test on Pierre I shale, with a drainage length $h$ = 19 mm (lateral drainage on 38 mm standard triaxial device). These values are to be compared with the values adopted on the COx claystone mentioned above: $6.5\times10^{-6}$ $s^{-1}$ by *Zhang and Rothfuchs (2004)* on 40 mm diameter and 80 mm high specimens, $1.0\times10^{-7}$ $s^{-1}$ and $0.9\times10^{-7}$ $s^{-1}$ by *Hu et al. (2014)* and *Menaceur et al. (2015)*, respectively, with 10 mm drainage length.

Theoretical estimations of the rate ensuring satisfactory drainage in standard triaxial tests were first made by *Gibson and Henkel (1954)* on clays, based on the theory of consolidation. *Monfared et al. (2011a)* carried out some numerical calculations to estimate excess pore pressures in a hollow cylindrical specimen of Opalinus Clay with a drainage length of 10 mm, determining a loading rate of 0.5 kPa/min to ensure satisfactory drained conditions. The same rate was found by *Belmokhtar et al (2017a)* in isotropic compression tests with a 10 mm drainage length.

Based on these results, the excess pore pressure during a shear test was estimated by considering an ideal isotropic linear saturated poroelastic material and by solving the set of coupled hydromechanical equations (1) to (6) by using the finite element method (2D FreeFem++ code, Hecht, 2012).

$$\nabla.\sigma + f = 0 \tag{1}$$

$$\nabla.q_w + \frac{\partial m_w}{\partial t} = 0 \tag{2}$$

$$q_w = -\rho_w \frac{k}{\mu_w} \nabla p_w \tag{3}$$

Eq. (1) is the balance of momentum in which $\sigma$ is the total stress and $f$ the gravity forces, that are neglected. Eq. (2) is the water mass conservation in which $q_w$ is the water flux, $m_w$ the water mass and $t$ the time. The water flux is given by Darcy's law in Eq. (3), where $\rho_w$ is the water density, $k$ the intrinsic permeability, $\mu_w$ the water dynamic viscosity and $p_w$ the pore water pressure.

The stress strain relation is provided in Eq. 4:

$$\underline{d\varepsilon} = \underline{\underline{S}}\,(\underline{d\sigma} - b\underline{dp_w}) \tag{4}$$

where $d\varepsilon$ is the strain tensor, $d\sigma$ the stress tensor, $b$ the isotropic Biot coefficient and $S$ the isotropic linear elastic compliance tensor, defined by the Young's modulus $E$ and the Poisson coefficient $\nu$ as follows:

$$\underline{\underline{S}} = \begin{pmatrix} \frac{1}{E} & \frac{-\nu}{E} & \frac{-\nu}{E} \\ \frac{-\nu}{E} & \frac{1}{E} & \frac{-\nu}{E} \\ \frac{-\nu}{E} & \frac{-\nu}{E} & \frac{1}{E} \end{pmatrix} \tag{5}$$

Within a poroelastic framework (*Coussy 2007; Ghabezloo et al. 2008*), one can also express the porosity $\phi$ with respect to the volumetric strain $\varepsilon_v$, the Biot Skeleton modulus $N$ and the pore water pressure $p_w$ as follows:

$$d\phi = -bd\varepsilon_v + \frac{1}{N}dp_w,\ \frac{1}{N} = \frac{b-\phi_0}{K_s} \tag{6}$$

The Young's modulus $E$ and Poisson ratio $\nu$ of the COx claystone were taken as 4 GPa and 0.3 respectively (*Gens et al., 2007*), providing a drained bulk modulus $K_d$ of 3.3 GPa. The unjacketed bulk modulus $K_s$ was taken as 21.7 GPa (*Belmokhtar et al., 2017a*), resulting in a Biot coefficient $b$ of 0.84 (with $b = 1 - K_d/K_s$). An isotropic permeability coefficient $k = 4\times20^{-20}$ m$^2$ and a porosity $\phi = 18\%$ were adopted (Gens et al. 2007; Charlier et al. 2013). The bulk water compression modulus and dynamic viscosity at 25°C were taken $K_w = 2237$ MPa and $\mu_w = 8.9\times10^{-10}$ MPa.s, respectively (Spang, 2002).

The pore pressure calculations were made by using an axisymmetric configuration, with drainage boundary conditions corresponding to the enhanced drainage system (Figure 2), described in more detail in Figure 4a. As seen in the Figure, a water pressure of 4 MPa is applied on the top and upper right lateral face of the specimen, whereas no water transfer is allowed on a small area in the lower lateral face, in a zone where the membrane is in direct contact with

the specimen. A comparison is also made by running calculations with drainage only on the top of the specimen (Figure 4b).

Four axial strain rates were considered: $6.6\times10^{-8}$ s$^{-1}$ (0.3 μm/mn), $1.1\times10^{-7}$ s$^{-1}$ (0.5 μm/mn), $2.2\times10^{-7}$ s$^{-1}$ (1 μm/mn) and $1.1\times10^{-6}$ s$^{-1}$ (5 μm/mn). The effect of the axial strain rate on the generated excess pore pressure is presented in Figure 5a in the case of enhanced lateral drainage. The pore pressure profiles are typical of pore pressure dissipation curves calculated with Terzaghi's consolidation theory, with maximum value at mid height.

Unsurprisingly, the lowest excess pore pressure (50 kPa) is obtained at the lowest strain rate of $6.6\times10^{-8}$ s$^{-1}$ (0.3 μm/mn), whereas an excess pore pressure of 630 kPa is observed at the fastest rate of $1.1\times10^{-6}$ s$^{-1}$. The comparison between enhanced and standard drainage conditions at lowest rate of $6.6\times10^{-8}$ s$^{-1}$ (Figure 5b) confirms the efficiency of the lateral drainage.

Figure 5c shows the changes in excess pore pressure with respect to the increment of shear stress $dq = d(\sigma_1 - \sigma_3)$ where $\sigma_1$ is the axial stress and $\sigma_3$ is the (constant) radial one. Compared to the top and bottom drainage condition where the excess pore pressure reaches a value of 370 kPa with no stabilisation, stabilisation is more rapidly reached with lateral drainage at a value of 50 kPa, once $dq$ reaches 0.6 MPa. 50 kPa is an acceptable value that can be neglected given the values of peak stress in claystones. Note that this is also true for the value of 80 kPa obtained at $1.1\times10^{-7}$ s$^{-1}$ (0.5 μm/mn). Figure 5c also shows that the steady state is not reached during the first stage of loading at the centre of the specimen with drainage at the top and bottom only, which can result in a wrong elastic modulus.

The satisfactory results obtained with these calculations at a rate of $6.6\times10^{-8}$ s$^{-1}$ are comparable with the values of strain rate adopted in claystones and shales by Wu et al. (1997) and Islam and Skalle (2013), equal to $3\times10^{-8}$ s$^{-1}$ and $2\times10^{-8}$ s$^{-1}$, respectively. They are around two orders of magnitude smaller than those used by *Zhang and Rothfuchs (2004)* and *Masri et al. (2014)* ($6.5\times10^{-6}$ s$^{-1}$ and $1.0\times10^{-6}$ s$^{-1}$, respectively) and approximately correspond to half the values adopted by *Hu et al. (2015)* and *Menaceur et al. (2016a)* on devices with smaller drainage lengths ($1.0\times10^{-7}$ s$^{-1}$ and $0.9\times10^{-7}$ s$^{-1}$ with a 10 mm drainage length) .

## 3. Experimental results and discussion

### 3.1. Drained test on Rothbach sandstone

Prior to testing a low permeability material, the reliability of the system with respect to the quality and accuracy of strain measurements was first checked by running a drained isotropic compression test at a stress rate of 50 kPa/min on Rothbach sandstone, a sandstone

composed of 85% quartz, 12% feldspars and 3% clays, with a porosity of 16% (*Ghabezloo and Sulem, 2009)* and a permeability of $5\times10^{-13}$ $m^2$ (*Ferfera 2001*). *Ghabezloo and Sulem (2009, 2010)* determined the unjacketed modulus of the Rothbach sandstone (41.6 GPa) and saw a significant stress dependency of its drained bulk modulus, that increased from 2 to 10 GPa when the effective confining stress was increased from 2 to 13 MPa. The Skempton *B* coefficient decreased from 0.75 to 0.55 for an effective confining pressure increase from 1.5 to 5 MPa. Over the same range of pressure, the undrained bulk modulus increased from about 8 to 16 GPa.

Given that, in this work, the isotropic compression test was run by injecting confining fluid in the cell, it was found easier to control a confinement loading rate rather than a strain loading rate. Assuming a mean drained bulk modulus of about 5 GPa (see *Ghabezloo and Sulem, 2009*), one can estimate the volumetric strain rate at about $1.6\times10^{-7}$ $s^{-1}$, corresponding to a value of $5.5\times10^{-8}$ $s^{-1}$ for both radial and axial strain rates. Various loading-unloading drained cycles were performed by cycling the confining stress between 2 MPa and 15 MPa with a constant pore pressure of 1 MPa.

The results obtained are plotted together with that of *Ghabezloo and Sulem (2009)* in Figure 6. The close values of radial and axial strains measured demonstrate the isotropic nature of the sandstone. The volumetric response during the loading phase appears to be quite comparable to that provided by *Ghabezloo and Sulem (2009)*, confirming the stress dependent feature and the non-linearity of the drained bulk modulus of the Rothbach sandstone. This good correspondence provides good confidence in the quality of the strains measurements.

### 3.2. Saturation of the COx claystone specimens

As mentioned in the introduction, the COx claystone is very sensitive to changes in water content and partially saturated states are known to provide higher Young's modulus and strength (*Zhang and Rothfuchs 2004; Pham et al. 2007, Menaceur et al. 2015*). As commented above, the specimens trimmed from the cores in the laboratory were not fully saturated. To properly test the mechanical behaviour of low permeability geo-materials, particular attention should be devoted to the resaturation procedure prior to mechanical testing. Following *Monfared et al. (2011a)* on the Opalinus clay and *Mohajerani et al. (2011), Menaceur et al. (2015; 2016a)* and *Belmokhtar et al. (2017a)* on the COx claystone, saturation was performed under stress conditions close to in-situ ones in an attempt to minimize swelling. To do so, any contact of the specimen with water was avoided by keeping the circuits and the porous elements (geotextile and porous stones) dry during the specimen setup. Then, the specimen surrounded

by geotextile (Figure 3a) was placed on the base, the membrane was placed and the LVDTs fixed to the specimen. The cell was then placed and filled with the confining fluid (oil). Vacuum was applied through the valve located close to the pressure transducer (PT) so as to evacuate any trapped air between the membrane and the specimen while maintaining closed the valves situated between water PVCs and the cell ducts. The confining stress was increased to 8 MPa, a value close to the value of the in-situ Terzaghi mean effective stress $\sigma'$ ($\sigma' = \sigma - p_w$) estimated by Wileveau et al. (2007). The drainage system under vacuum was then filled with de-aired water through the PT valves while the PVC valves were kept closed, ensuring good saturation of the drainage system in a first stage, and of the specimen in a second stage. Note that the desaturation of the claystone ($S_r$ = 87.9%) from the initial saturated state resulted in a slight increase in salinity, that was compensated by the specimen resaturation with demineralized water. Finally, the confining stress and pore pressure were simultaneously increased up to 12 MPa and 4 MPa, respectively, at a rate of 100 kPa/min, to reach stress conditions close to in-situ. The use of high back pressure is also recommended to ensure air bubbles dissolution in pore fluid when saturating low permeability shales (Wu et al., 1997).

Figure 7 shows the monitored radial local strain $\varepsilon_2$ (parallel to bedding) and axial local strain $\varepsilon_1$ (perpendicular to bedding) together with the volumetric strain ($\varepsilon_v = \varepsilon_1 + 2\varepsilon_2$). A clear anisotropy is observed, with axial swelling larger than the radial one in both specimens. The measured strains stabilize after a period of 8 days in specimen EST51338a and 10 days in specimen EST51338b. The monitored volumetric swelling strains is about 0.97% in specimen EST51338a and 0.85% in specimen EST51338b, comparable to the volumetric strain (1.11%) measured by *Menaceur et al. (2015)*. Unfortunately, no comparison could be made with the volume changes calculated from the water absorbed by the specimen through the back-pressure PVCs, because of a leak that occurred somewhere in the connecting lines between the specimen and the PVCs. As observed in Figure 7, the water exchange curves are linear in both cases, with no final stabilisation, unlike the local strain measurements.

Because of this leak, no determination of the Skempton *B* parameter could be made by increasing the confining stress, since the pore pressure measurement was affected by the leak in the back-pressure circuit. Note however that *Mohajerani et al. (2011) and Belmokhtar et al. (2017)* obtained, on the same claystone under the same stress conditions ($\sigma$ = 12 MPa and $p_w$ = 4 MPa), a Skempton coefficient (B = 0.84) corresponding to full saturation, with a 10 mm drainage length, in tests in which the stabilisation of volume changes occurred after 3 days. So,

it is considered that the stabilisation reached here after 15 days with a drainage length of 19 mm should also correspond to full saturation.

### 3.3. Shear tests

Two shear tests were conducted on specimens EST51338a and EST51338b along two different loadings paths (Figure 8) at a temperature of 25°C. Both specimens were saturated under a Terzaghi effective stress $\sigma'$ close to the in-situ effective stress ($\sigma'$ = 8 MPa, $\sigma_3$ = 12 MPa, $p_w$ = 4 MPa). Specimen EST51338a was sheared under in-situ effective stress, and specimen EST51338b was sheared at 1.5 in-situ effective stress ($\sigma'$ = 12 MPa, $\sigma_3$ = 16 MPa, $p_w$ = 4 MPa). The increase in confining stress until 16 MPa in test EST51338b was carried out with a loading rate of 0.5 kPa/min, small enough ensure drained conditions (*Monfared et al., 2011a; Menaceur et al., 2015; Belmokhtar et al., 2017a*).

The drained shear tests were carried out under constant confining stress with a strain rate of $6.6\times10^{-8}$ $s^{-1}$ (0.3 μm/min) to ensure satisfactory drainage conditions. The axial strength was measured with both internal and external force gauges, that provided similar responses.

The shear tests results are presented in Figure 9 in terms of radial, axial and volumetric strain changes with respect to the differential stress ($q_d = \sigma_1 - \sigma_3$) for the two confining stresses. The stress-strain curves are typical of claystones, with similar contraction-dilation in both cases. For specimen EST51338a under stress conditions close to in-situ, the transition from contraction to dilation is observed at a differential stress of 14.4 MPa and the peak is reached at $q_d$ = 18,2 MPa, at 1.28% axial and – 0.67% radial strain (- 0.06% volumetric strain). The same occurs for test EST51338b under 12 MPa confining stress, with a transition from contraction to dilation at $q_d$ = 17 MPa prior to reaching peak at $q_d$ = 22,2 MPa, at 1.32% axial and – 0.73% radial strain (- 0.14% volumetric strain). In both cases, the externally measured axial strain is higher than the local one, confirming the interest of local measurements.

The post-peak response is governed by the creation of a shear plane with an inclination of about 65° with respect to horizontal, as shown in Figure 10. These results are comparable to other ones obtained in claystones by *Naumann et al. (2007), Zhang et al. (2007), Hu et al. (2014)* and *Menaceur et al. (2015).* As expected, the mechanical response is stress dependent with higher shear strength at higher confining stress, giving a value of stress at peak equal to 18 MPa at 8 MPa effective confining stress and 22 MPa at 12 MPa effective confining stress.

The values of shear strength are plotted together in a *q-p'* diagram together with the results of *Hu et al. (2014)* on small specimens and *Menaceur et al. (2015)* in the hollow cylinder

apparatus (Figure 11). Given that the numerical calculations conducted by *Monfared et al. (2011)* showed that the strain rate (0.9 x $10^{-7}$ $s^{-1}$) adopted by *Menaceur et al. (2015)* with a drainage length of 10 mm in the hollow cylinder apparatus ensured good drainage conditions, and given that *Hu et al. (2014)* adopted a comparable strain rate (1 x $10^{-7}$ $s^{-1}$) with the same drainage length, all data correspond to drained conditions. One observes a good overall comparability of the drained shear strength data obtained on various devices, with parallel curves that provide the same value of friction angle of 21°. Shear strength values are also well related with respect to the specimen's porosities, with the largest strength at lower porosity of 13% (Hu et al. 2014, Menaceur et al. 2015) and smallest one at the highest porosity of 17% (Menaceur et al. 2015).

The shear stress/axial strain curves of Figure 9 allow one to determine some elastic parameters at various Terzaghi effective stresses ($\sigma'$). The strain-stress relationship for a transversely isotropic material in drained conditions is given by *Detournay and Cheng (1993)* as follows:

$$\begin{pmatrix} d\varepsilon_1 \\ d\varepsilon_2 \\ d\varepsilon_2 \end{pmatrix} = \begin{pmatrix} \frac{1}{E_1} & \frac{-\nu_{12}}{E_1} & \frac{-\nu_{12}}{E_1} \\ \frac{-\nu_{12}}{E_1} & \frac{1}{E_2} & \frac{-\nu_{23}}{E_2} \\ \frac{-\nu_{12}}{E_1} & \frac{-\nu_{23}}{E_2} & \frac{1}{E_2} \end{pmatrix} \begin{pmatrix} d\sigma_1 \\ d\sigma_2 \\ d\sigma_2 \end{pmatrix} \tag{7}$$

where, $E_1$ is the Young's modulus in the direction $x_1$ perpendicular to bedding plane, $E_2$ the Young's modulus in the direction $x_2$ parallel to bedding plane, $\nu_{12}$ and $\nu_{23}$ are the Poisson ratios in the ($x_1$, $x_2$) and ($x_2$, $x_3$) planes, respectively. In a case of drained shearing test with constant radial stress, the measurement of axial and radial strains allows one to determine the Young's modulus $E_1$ and the Poisson's ratio $\nu_{12}$ using the following relations:

$$\frac{d\varepsilon_1}{d\sigma_1} = \frac{1}{E_1} \tag{8}$$

$$\frac{d\varepsilon_2}{d\sigma_1} = \frac{-\nu_{12}}{E_1} \tag{9}$$

A Young's secant modulus $E_1$ = 2.9 GPa is obtained from the data of Figure 9a at 0.1% axial strain under a Terzaghi effective stress close to in-situ ($\sigma'$ = 8 MPa), with a $\nu_{12}$ Poisson's ratio of 0.22. Under a 12 MPa Terzaghi effective stress, a larger Young's modulus

$E_1$ of 4.2 GPa is obtained with a Poisson's ratio $\nu_{12} = 0.14$. These parameters are summarized in Table 2.

The Young's moduli obtained with a porosity of 16% are in good agreement with that obtained by *Menaceur et al. (2015)* with a porosity of 17%, confirming also the rate of increase in $E_1$ with effective stress (Figure 12a). The Young's modulus obtained by *Menaceur et al. (2015)* at 8 MPa Terzaghi effective stress at a porosity of 13% is slightly higher than that obtained in this study. The agreement between both data sets is however not observed in terms of change in Poisson's ratio with stress (Figure 12b), with a decrease obtained here compared with the increase observed by *Menaceur et al. (2015)*. Note however that the measurement of the Poisson's ratio is rather difficult because of the small range of the measured radial strains and of the uncertainties in measurements.

These data confirm that, provided that a sufficiently low axial strain rate is adopted, the drained triaxial system developed with standard triaxial specimens (38 mm diameter and 76 mm height) in this work provides on low permeability shales comparable results than other enhanced drained triaxial devices.

The mechanical properties of the COx claystone presented here, together with those of *Hu et al. (2014)* and *Menaceur et al. (2016a)*, were all obtained after resaturating the specimens under stress. Whereas *Hu et al. (2014)* imposed a confining stress of 2 MPa and a pore pressure of 1 MPa, *Menaceur et al. (2016a)* performed their resaturation under larger stress (9 MPa confining stress, 1 MPa pore pressure), close to the in-situ value of the Terzaghi effective stress. The same effective stress was adopted here, with a confining stress of 12 MPa and a pore pressure of 4 MPa, closer to in-situ stress conditions. In all cases, some swelling of the specimens, generally close to 1 %, was observed during the resaturation procedure. Such swelling could perhaps result in some damage and an underestimation of the mechanical characteristics of the specimens, given that swelling occurs through the developments of micro-cracks (*Wan et al. 2013, Wang et al. 2013, Menaceur et al. 2016b*). Indeed, the values obtained here are smaller than those provided by *Andra (2005)* and *Armand et al. (2016)*, in which an average value of the Young modulus of 6 GPa is considered as representative of the clayey layer at the level of the Bure URL. Similarly, the failure criterion presented in *Armand et al. (2016)* is reasonably parallel to the criterion of Figure 11, but with larger stresses at failure, with an intersection with the $q$ axis comprised between 12 and 20 MPa. Note that the tests reported in Armand et al. (2016) have been conducted at an axial strain rate of $10^{-6}$ $s^{-1}$ on standard triaxial specimens previously equilibrated under a relative humidity of 90% (suction

13.1 MPa). This resulted in a water content of 6% and a degree of saturation estimated around 95%, based on existing data on the retention properties of the COx claystone (*Wan et al. 2013*). The combined effects of these testing conditions on the failure stress obtained should then be further investigated, given that partial saturation and high axial strain rate could also have some effects on the measured mechanical parameters. Of course, the best way to determine a representative set of parameters could be to avoid the resaturation procedure by testing fully saturated specimens, and all the possible ways of minimising desaturation during coring, storage and specimen trimming should be looked for prior testing the specimens in the laboratory.

## 4. Conclusion

To cope with the difficulty of running drained triaxial tests in low permeability claystones and shales, a drainage system enhanced by using upper and lower geotextiles placed around a standard triaxial specimen, and respectively connected to the upper and lower porous stones was developed. Besides reducing the drainage length to the specimen radius (19 mm), the system produced satisfactory resaturation thanks to the absence of a connection between the geotextiles, forcing water infiltration (connected geotextiles would have worked as a by-pass between the top and bottom porous stones). High precision in radial strain measurements were made possible by ensuring direct contact between the LVDT stems and the specimen through the membrane.

Particular attention was paid to the saturation phase that has been conducted under high confining and back pressures to avoid any possible damage and to ensure full dissolution of air bubbles into the pore water.

An isotropic compression validation test was carried out on a Rothbach sandstone providing a volumetric response comparable to *Ghabezloo and Sulem (2009)*, providing good confidence in the quality of the strain measurements.

Finally, based on a poroelastic coupled calculation, the axial strain rates necessary to ensure full drainage conditions was estimated. A strain rate of $6.6\times10^{-8}$ $s^{-1}$ was adopted and two shear tests were conducted on specimens of the COx claystone under in-situ effective stress condition ($\sigma$ = 12 MPa, $p_w$ = 4 MPa) and 1.5 in-situ effective stress condition ($\sigma$ = 16 MPa, $p_w$ = 4 MPa). The peak shear stresses obtained are located along a failure line reasonably parallel to the failure envelope previously obtained by *Hu et al. (2014)* and *Menaceur et al. (2015)*. The envelope obtained corresponds to smaller shear strength values compared to what

are considered to be the characteristic values of the COx claystone (*Andra 2005*, *Armand et al*. *2016)*. This could be due to possible under-estimation of the parameters that result from the 1% swelling observed during the saturation phase under stress. Conversely, the effects of testing specimens previously submitted to a controlled relative humidity that result in an almost saturated state should also be further considered.

Compared to other methods of triaxial testing with reduced drainage length, the device developed here has the advantage to be easier to use compared to the hollow cylinder developed by *Monfared et al*. *(2011)*. Compared to the small specimens tested by *Hu et al*. *(2014)*, the use of standard triaxial specimens allows for having high precision local measurements of axial and radial strains, made possible here by ensuring direct contact of the LVDT rods with the specimen. This capability is of great importance with respect to the determination of the elastic parameters that requires the measurement of small strains along reversible stress paths.

**Acknowledgements**

The authors are indebted to Andra, the French agency for the management of radioactive wastes, for funding this work, providing the claystone specimens and for fruitful discussions. The work was also supported by Ecole des ponts ParisTech, in the framework of the PhD thesis of the first author. The detailed examination and fruitful suggestions by the Co-editor and the anonymous Reviewer also helped for significantly improving this contribution.

## References


Andra (2005) Synthesis argile: evaluation of the feasibility of a geological repository in argillaceous formation.

Aoki T, Tan CP, Cox RHT, Bamford WE (1995) Determination ofanisotropic poroelastic parameters of a transversely isotropic shale by means of consolidated undrained triaxial tests. Proc. 8th Int. Cong. Rock Mech. T. Jujii Ed, Tokyo, Japan, 2, 172-176.

Belmokhtar M, Delage P, Ghabezloo S, Menaceur H, Tang AM, Conil N (2017a) Poroelasticity of the Callovo–Oxfordian Claystone. Rock Mech Rock Eng 50:871–889. doi: 10.1007/s00603-016-1137-3

Belmokhtar M, Delage P, Ghabezloo S, Conil N (2017b) Thermal Volume Changes and Creep in the Callovo-Oxfordian Claystone. Rock Mech Rock Eng. doi: 10.1007/s00603-017-1238-7

Bishop AW, Henkel DJ (1957) The measurement of soil properties in the triaxial test. Edward Arnold (Publishers) LTD, London

Bonini M, Debernardi D, Barla M, Barla G (2009) The Mechanical Behaviour of Clay Shales and implications on the Design of Tunnels. Rock Mech Rock Eng 42(2): 361-388.

Busch A, Alles S, Gensterblum Y, Prinz D, Dewhurst D, Raven M, et al. (2008) Carbon dioxide storage potential of shales. Int J. Greenh Gas Control 2(3):297–308.

Charlier R, Collin F, Pardoen B, Talandier J, Radu JP, Gerard P (2013) An unsaturated hydro-mechanical modelling of two in-situ experiments in Callovo-Oxfordian argillite. Eng Geol 165:46–63.

Chiarelli AS (2000) Étude expérimentale et modélisation du comportement mécanique de l'argilite de l'est. PhD thesis, Université Lille I.

Chiarelli AS, Shao JF, Hoteit N (2003) Modeling of elastoplastic damage behavior of a claystone. Int J Plast 19:23–45.

Chiu HK, Johnston IW, Donald IB (1983) Appropriate Techniques for Triaxial Testing of Saturated Soft Rock. Int J Rock Mech Mining Sc & Geomech Abst 20(3):107-120

Coussy O (2007) Revisiting the constitutive equations of unsaturated porous solids using a Lagrangian saturation concept. 1675–1694.

Davy CA, Skoczylas F, Barnichon J-D, Lebon P (2007) Permeability of macro-cracked argillite

under confinement: Gas and water testing. Phys Chem Earth, Parts A/B/C 32:667–680.

Delage P, Cui YJ, Tang a M (2010) Clays in radioactive waste disposal. J Rock Mech Geotech Eng 2:111–123. doi: 10.3724/SP.J.1235.2010.00111

Delage P, Menaceur H, Tang A-M, Talandier J (2014) Suction effects in deep Callovo-Oxfordian claystone Suction effects in deep Callovo-Oxfordian claystone. Géotechnique Lett 4:267–271.

Detournay E, Cheng AH (1993) Fundamentals of Poroelasticity. Chapter 5 Compr Rock Eng Princ Pract Proj Vol II, Anal Des Method, ed C Fairhurst, Pergamon Press II:113–171.

Einstein HH (2000) Tunnels in Opalinus Clayshale: A Review of Case Histories and New Developments. Tunnelling and underground space technology 15(1): 13-29.

Escoffier S (2002) Caractérisation expérimentale du comportement hydromécanique des argilites de Meuse Haute-Marne. PhD thesis, Institut National Polytechnique de Lorraine.

Eseme E, Urai JL, Krooss BM, Littke R (2007) Review of mechanical properties of oil shales: implications for exploitation and basin modelling. Oil Shale 24(2):159–174

Ewy RT, Stankovich RJ, Bovberg CA (2003) Mechanical Behavior of Some Clays and Shales from 200m to 3800m Depth. In: Culligan P, Einstein H, Whittle A (eds) Soil and Rock America 2003: Proc. 12th PanAm Conf Soil Mech Geotech Eng and 39th US Rock Mech Symp. Verlag Glückauf, Essen, 445-452.

Ewy RT (2015) Shale/claystone response to air and liquid exposure, and implications for handling, sampling and testing. Int J Rock Mech Min Sci 80:388–401.

Ferfera FMR (2001) Mécanismes physiques de l'évolution de la perméabilité d'un grès sous chargements simulant la déplétion d'un gisement. Oil Gas Sci Technol 56:347–355. doi: 10.2516/ogst:2001030

Gaucher E, Robelin C, Matray JM, Négrel G, Gros Y, Heitz JF, Vinsot A, Rebours H, Cassagnabère A, Bouchet A (2004) ANDRA underground research laboratory: Interpretation of the mineralogical and geochemical data acquired in the Callovian-Oxfordian formation by investigative drilling. Phys Chem Earth 29:55–77.

Gens A, Vaunat J, Garitte B, Wileveau Y (2007) In situ behaviour of a stiff layered clay subject to thermal loading : observations and interpretation. Géotechnique 57:207–228.

Ghabezloo S, Sulem J, Guédon S, Martineau F, Saint-Marc J (2008) Poromechanical behaviour

of hardened cement paste under isotropic loading. Cem Concr Res 38:1424–1437.

Ghabezloo S, Sulem J (2009) Stress dependent thermal pressurization of a fluid-saturated rock. Rock Mech Rock Eng 42:1–24.

Ghabezloo S, Sulem J (2010) Effect of the volume of the drainage system on the measurement of undrained thermo-poro-elastic parameters, Int. J. Rock Mech. Min. Sci., 47, 60–68.

Gibson RE, Henkel DJ (1954) Influence of Duration of tests at Constant Rate of Strain on Measured "Drained" Strength. Géotechnique 4:6–15.

Hecht F (2012) New development in freefem+. J Numer Math 20:251–265. doi: 10.1515/jnum-2012-0013

Hu DW, Zhang F, Shao JF (2014) Experimental study of poromechanical behavior of saturated claystone under triaxial compression. Acta Geotech 9:207–214.

Islam MA, Skalle P (2013) An experimental investigation of shale mechanical properties through drained and undrained test mechanisms. Rock Mech Rock Eng 46:1391–1413. doi: 10.1007/s00603-013-0377-8

Masri M, Sibai M, Shao JF, Mainguy M (2014) Experimental investigation of the effect of temperature on the mechanical behavior of Tournemire shale. Int J Rock Mech Min Sci 70:185–191.

Menaceur H, Delage P, Tang A-M, Conil N (2015) The thermo-mechanical behaviour of the Callovo-Oxfordian claystone. Int J Rock Mech Min Sci 78:290–303.

Menaceur H, Delage P, Tang A-M, Conil N (2016a) On the Thermo-Hydro-Mechanical Behaviour of a Sheared Callovo-Oxfordian Claystone Specimen with Respect to the EDZ Behaviour. Rock Mech Rock Eng 49:1875–1888.

Menaceur H., Delage P., Tang A.M. and Talandier J. 2016b. The status of water in swelling shales: an insight from the water retention properties of the Callovo-Oxfordian claystone. Rock Mech Rock Eng 49 (12), 4571- 4586

Mohajerani M, Delage P, Monfared M, Tang A-M, Sulem J, Gatmiri B (2011) Oedometric compression and swelling behaviour of the Callovo-Oxfordian argillite. Int J Rock Mech Min Sci 48:606–615.

Mohajerani M, Delage P, Sulem J, Monfared M, Tang A-M, Gatmiri B (2013) The Thermal Volume Changes of the Callovo–Oxfordian Claystone. Rock Mech Rock Eng 47:131–

142.

Mohajerani M, Delage P, Sulem J, Monfared M, Tang A-M, Gatmiri B (2012) A laboratory investigation of thermally induced pore pressures in the Callovo-Oxfordian claystone. Int J Rock Mech Min Sci 52:112–121.

Monfared M (2011) Couplages température-endommagement-perméabilité dans les sols et roches argileux. PhD thesis, Université Paris-Est.

Monfared M, Delage P, Sulem J, Mohajerani M, Tang A-M, De Laure E (2011a) A new hollow cylinder triaxial cell to study the behavior of geo-materials with low permeability. Int J Rock Mech Min Sci 48:637–649.

Monfared M, Sulem J, Delage P, Mohajerani M (2011b) A Laboratory Investigation on Thermal Properties of the Opalinus Claystone. Rock Mech Rock Eng 44:735–747. doi: 10.1007/s00603-011-0171-4

Naumann M, Hunsche U, Schulze O (2007) Experimental investigations on anisotropy in dilatancy, failure and creep of Opalinus Clay. Phys Chem Earth 32:889–895. doi: 10.1016/j.pce.2005.04.006

Pham QT, Vales F, Malinsky L, Nguyen M-D, Gharbi H (2007) Effects of desaturation–resaturation on mudstone. Phys Chem Earth, Parts A/B/C 32:646–655.

Schmitt L, Forsans T, Santarelli FJ (1994) Shale Testing and Capillary Phenomena, Int J Rock Mech Mining Sc & Geomech Abst, 31(5): 411-427.

Steiger RR, Leung RK 1991. Consolidated undrained triaxial test procedure for shales. Rock mechanics as a Multidisplinary Science, Proc. 32nd U.S. Syrup., JC Roegiers Ed: 637-646.

Spang B (2002) Excel add-in for properties of water and steam in SIunits. http://www.cheresources.com/iapwsif97.shtml.

Swan G, Cook J, Bruce S, Meehan R (1989) Strain rate effects in Kimmeridge bay shale. Int. J. Rock Mech. Min. Sci. & Geomech. Abstr, 26(2): 135-149.

Valès F, Nguyen Minh D, Gharbi H, Rejeb A (2004) Experimental study of the influence of the degree of saturation on physical and mechanical properties in Tournemire shale (France). Appl Clay Sci 26:197–207.

Villamor-Lora R, Ghazanfari E, Asanza Izquierdo E (2016) Geomechanical Characterization

of Marcellus Shale. Rock Mech Rock Eng, 49(9), 3403–3424.

Wan M, Delage P, Tang A-M, Talandier J (2013) Water retention properties of the Callovo-Oxfordian claystone. Int J Rock Mech Min Sci 64:96–104.

Wang L, Bornert M, Chanchole S (2013) Micro-scale experimental investigation of deformation and damage of argillaceous rocks under hydric and mechanical loads. Poromochanics V ASCE 1635–43.

Wileveau Y, Cornet FH, Desroches J, Blumling P (2007) Complete in situ stress determination in an argillite sedimentary formation. Phys Chem Earth 32:866–878. doi: https://doi.org/10.1016/j.pce.2006.03.018

Wissa AEZ (1969) Pore pressure measurement in saturated stiff soils. J. Soil Mech. Fdns Div. Am. Soc. civ. Engrs 95:SM4, 1063-1073.

Wu B, Tan CP, Aoki T (1997) Specially designed techniques for conducting consolidated undrained triaxial tests on low permeability shales. Int J Rock Mech Min Sci 34:336.e1-336.e14. doi: 10.1016/S1365-1609(97)00168-8

Yven B, Sammartino S, Geraud Y, Homand F, Villieras F (2007) Mineralogy, texture and porosity of Callovo-Oxfordian argilites of the Meuse/Haute-Marne region (eastern Paris Basin). Mémoires la société Géologique Fr 0249–7546:73–90.

Zhang CL (2011) Experimental evidence for self-sealing of fractures in claystone. Phys Chem Earth 36:1972–1980.

Zhang CL, Rothfuchs T (2004) Experimental study of the hydro-mechanical behaviour of the Callovo-Oxfordian argillite. Appl Clay Sci 26:325–336.

Zhang CL, Rothfuchs T, Su K, Hoteit N (2007) Experimental study of the thermo-hydro-mechanical behaviour of indurated clays. Phys Chem Earth, Parts A/B/C 32:957–965.

Zhang F, Xie SY, Hu DW, Gatmiri B (2012) Effect of water content and structural anisotropy on mechanical property of claystone. Appl Clay Sci 69:79–86.

**List of Tables**



**List of Figures**

Figure 6. Drained isotropic compression test carried out on Rothbach sandstone (porosity □ = 16%, permeability k = 5 x $10^{-3}$ $m^{-2}$), showing good comparability with the data of Ghabezloo and Sulem (2009).

Figure 7. Saturation phase: (a) EST51338a, (b) EST51338b. The volume changes could not be derived from the water volume absorbed by the specimen and monitored by the back-pressure PVCs, because of leaks in the back-pressure circuit, that resulted in having linear water exchanges in both cases.

Figure 8. Stress paths followed, with constant confining stress: a) Test on specimen EST51338a, submitted to an initial Terzaghi effective stress of 8 MPa, close to in-situ stress conditions; b) Test on specimen EST51338b, at 1.5 time the mean Terzaghi effective stress (12 MPa).

Figure 9. Stress strain curves of the drained sheared tests. Externally measured axial strains are in both cases larger than local ones. Similar contraction-dilation is observed in both cases, with a negative volumetric strain at peak (slight expansion); a) Specimen EST51338a under initial conditions close to in-situ mean effective stress (8 MPa); b) Specimen EST51338b under around 1.5 in-situ mean effective stress (12 MPa).

Figure 10. Sheared specimen (EST51338b), with shear plane inclined at an angle of 65° from horizontal.

Figure 11. Comparison of the shear envelopes determined in this work (porosity 16%) with data of shear tests determined with different devices on saturated specimens of the Callovo-Oxfordian claystone, with porosities between 12 and 17%: Menaceur et al. (2015) on hollow cylinder specimens; Hu et al. (2014) on small size triaxial specimens, either drained or undrained. Both devices had same drainage length (10 mm) with strain rates of 0.9×10-7 s-1 and 1.0×10-7 s-1, respectively. Shear envelopes are well organised with respect to the porosity.

Figure 12. Comparison of the elastic parameters determined in this work with those of Menaceur et al. (2015): a) Young's modulus, with good comparability between tests and a linear increase with the confining stress; b) Poisson's ratio, with poor comparability, probably due to the difficulties in accurately measuring this parameter due to the very small radial strains mobilised.

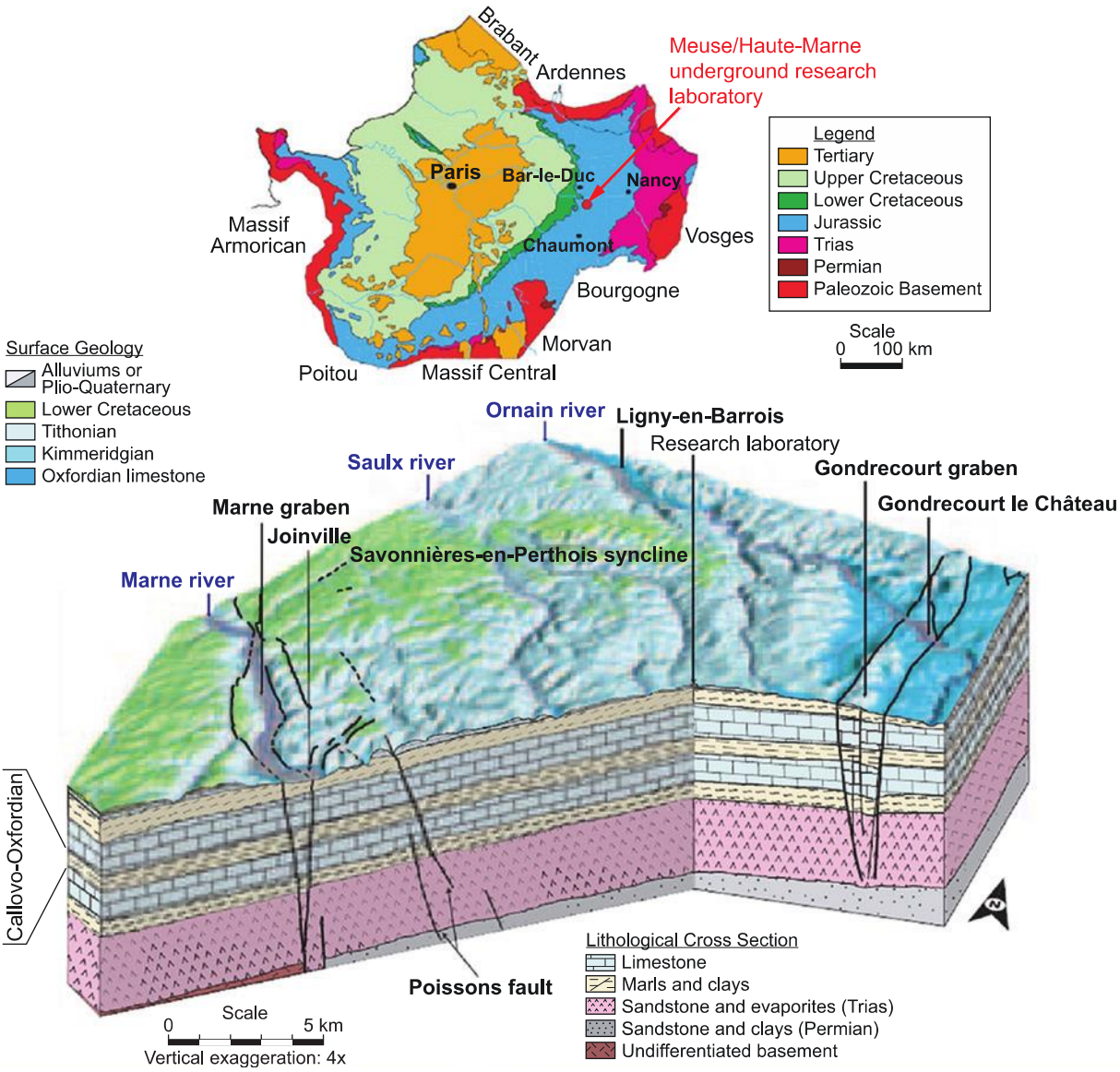


Figure 1. Geological map showing the location of the Bure underground research laboratory (also called Meuse-Haute Marne URL), located in the eastern area of the Paris sedimentary basin, at the boundary between two French departments, the Meuse and the Haute Marne departments. The layer of Callovo-Oxfordian claystone is located between two layers of limestone, at a depth of around 500 m (ANDRA 2005).

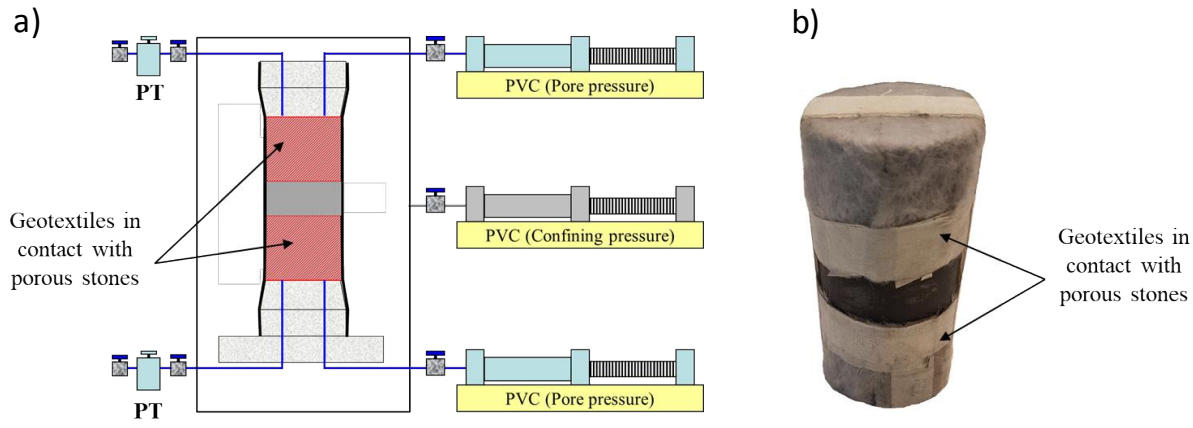


Figure 2. a) Overall schematic view of the specimen mounted with the 3 PVC connected: two PVCs are independently connected to the upper and lower geotextiles, respectively, whereas the third one is connected to the confining fluid (silicon oil) in the cell, so as to apply the confining stress; b) Photo of the specimen wrapped into the upper and lower geotextiles. Each geotextile is connected to the porous disks, placed on top and bottom of the specimen, respectively.

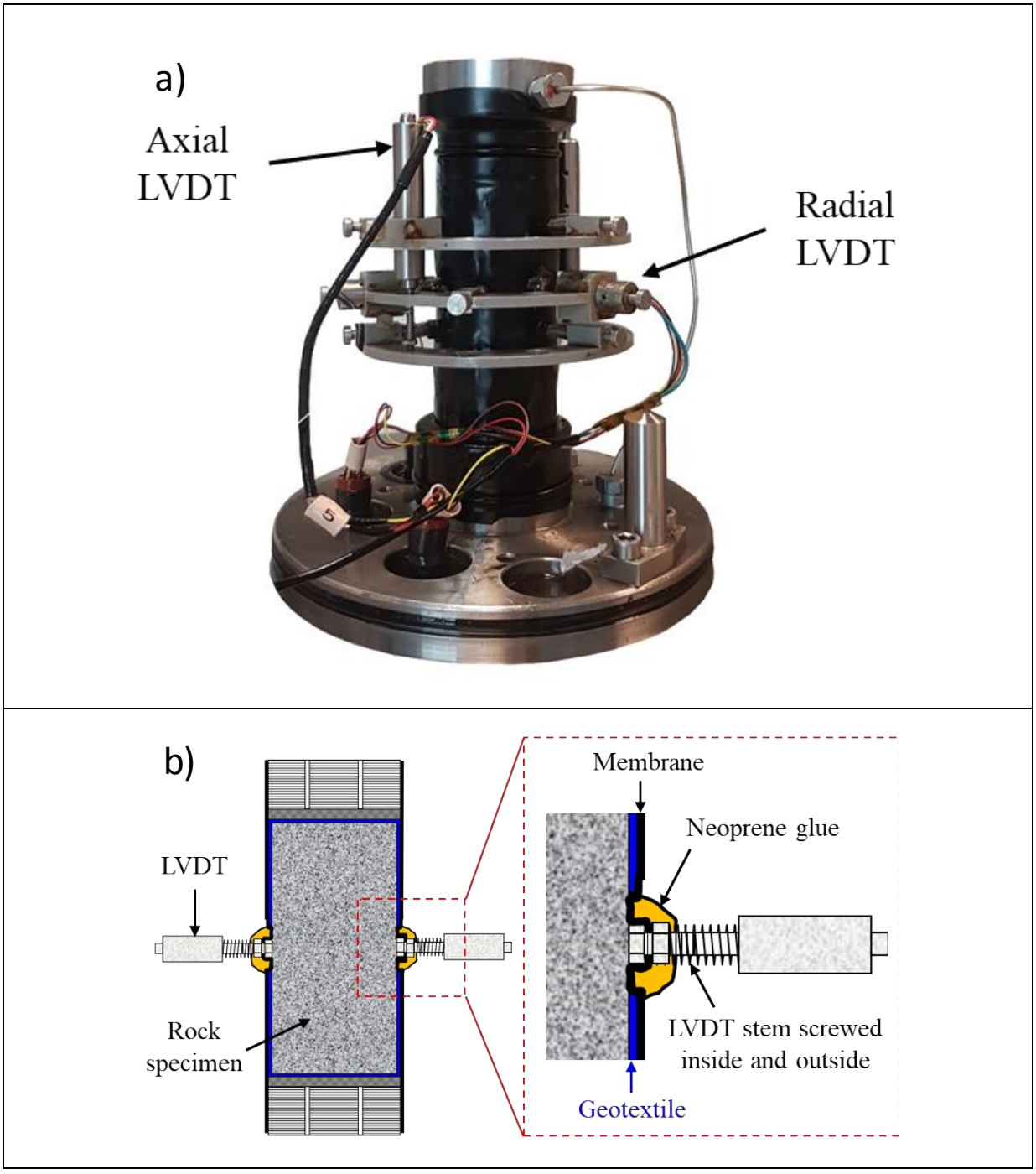


Figure 3. a) Local strain measurements device. Four radial LVDTS are fixed on a ring surrounding the specimen; the two axial LVDTs provide the changes in distance between two other rings tightly fixed on the specimen; b) Detail of the direct contact between the LVDT stem and the specimen through the neoprene membrane, with two bolts screwed on the stem on both sides of the membrane. Fluid tightness is ensured by a drop of neoprene glue put around the stem.

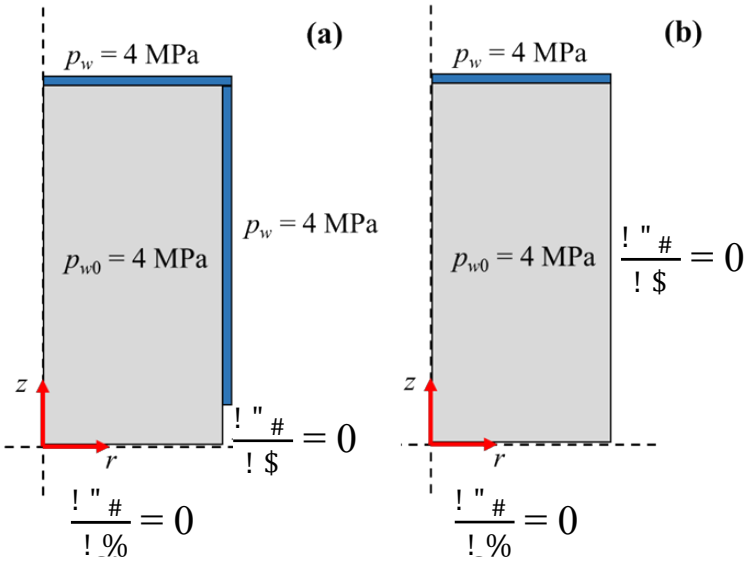


Figure 4. Initial and boundary conditions applied on a quarter upper right specimen in axisymmetric conditions: a) Enhanced drainage is made possible thanks to both the top porous disk and the lateral geotextile connected to it; b) Simple drainage by the top porous disk only.

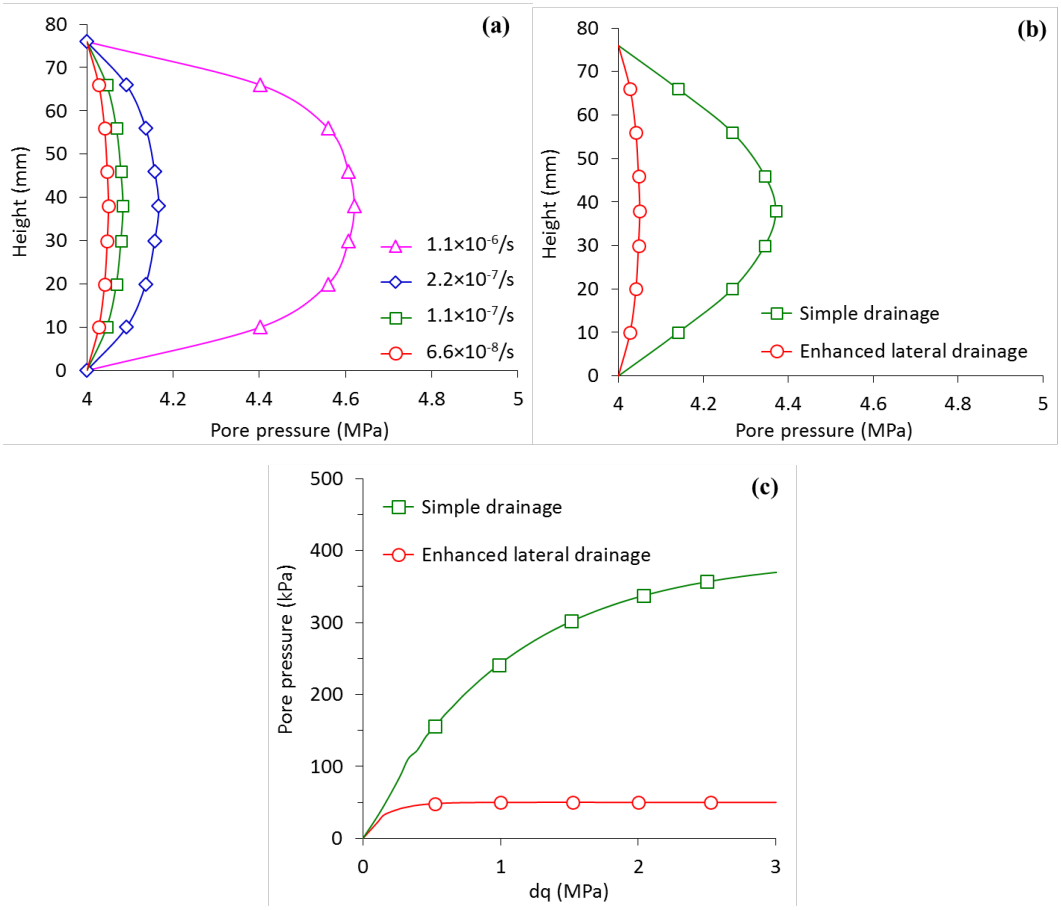


Figure 5. a) Calculated excess pore pressure profiles at steady state at different rates with enhanced lateral drainage, showing satisfactory drainage at strain rates of 6.6 x $10^{-8}$ and 1.1 x $10^{-7}$ $s^{-1}$; b) Comparison between simple and enhanced lateral drainage at a rate of $6.6\times10^{-8}$ $s^{-1}$; c) Pore pressure changes at the centre of the sample at a rate of $6.6\times10^{-8}$ $s^{-1}$, showing no stabilisation in pore pressure with simple drainage.

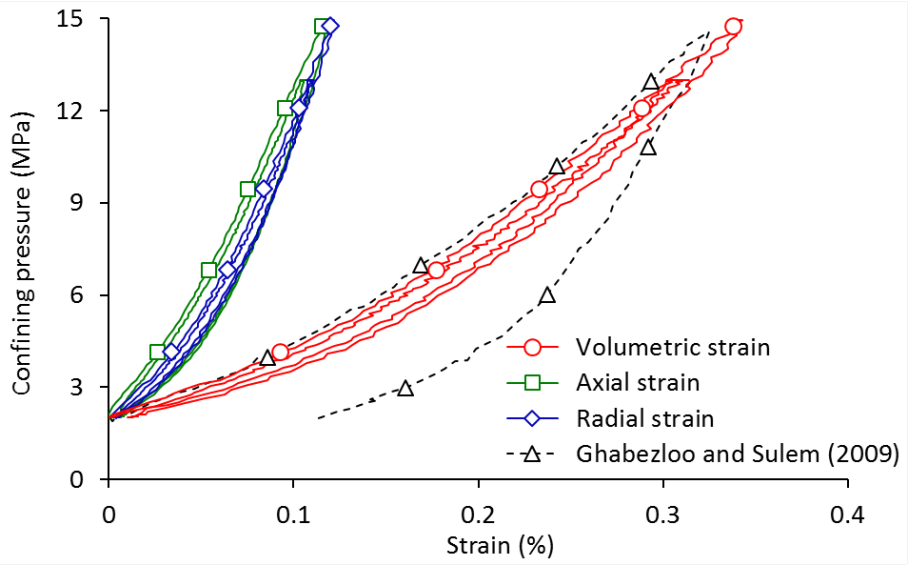


Figure 6. Drained isotropic compression test carried out on Rothbach sandstone (porosity $\phi$ = 16%, permeability $k$ = 5 x $10^{-3}$ $m^{-2}$), showing good comparability with the data of Ghabezloo and Sulem (2009).

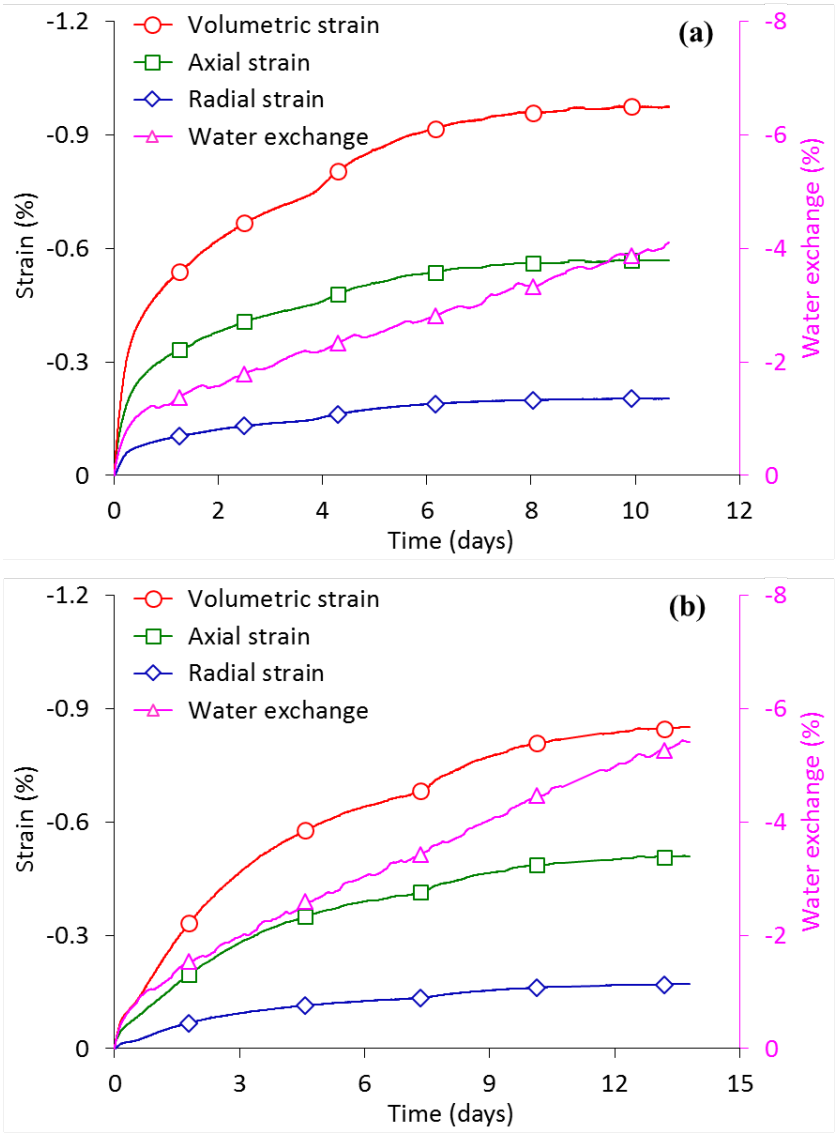


Figure 7. Saturation phase: (a) EST51338a, (b) EST51338b. The volume changes could not be derived from the water volume absorbed monitored by the back-pressure PVCs because of leaks in the back-pressure circuit, that resulted in having linear water exchanges in both cases.

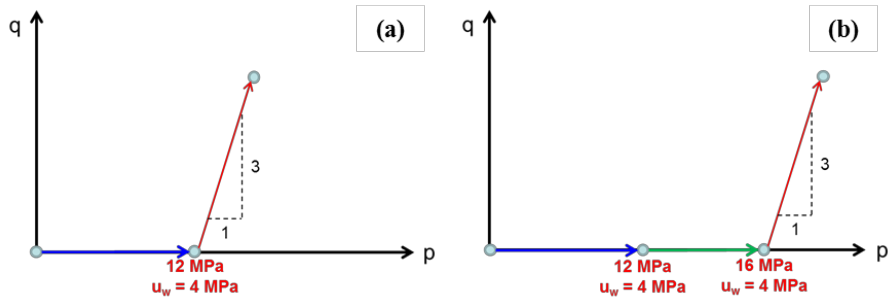


Figure 8. Stress paths followed, with constant confining stress: a) Test on specimen EST51338a, submitted to an initial Terzaghi effective stress of 8 MPa, close to in-situ stress conditions; b) Test on specimen EST51338b, at 1.5 time the mean Terzaghi effective stress (12 MPa).

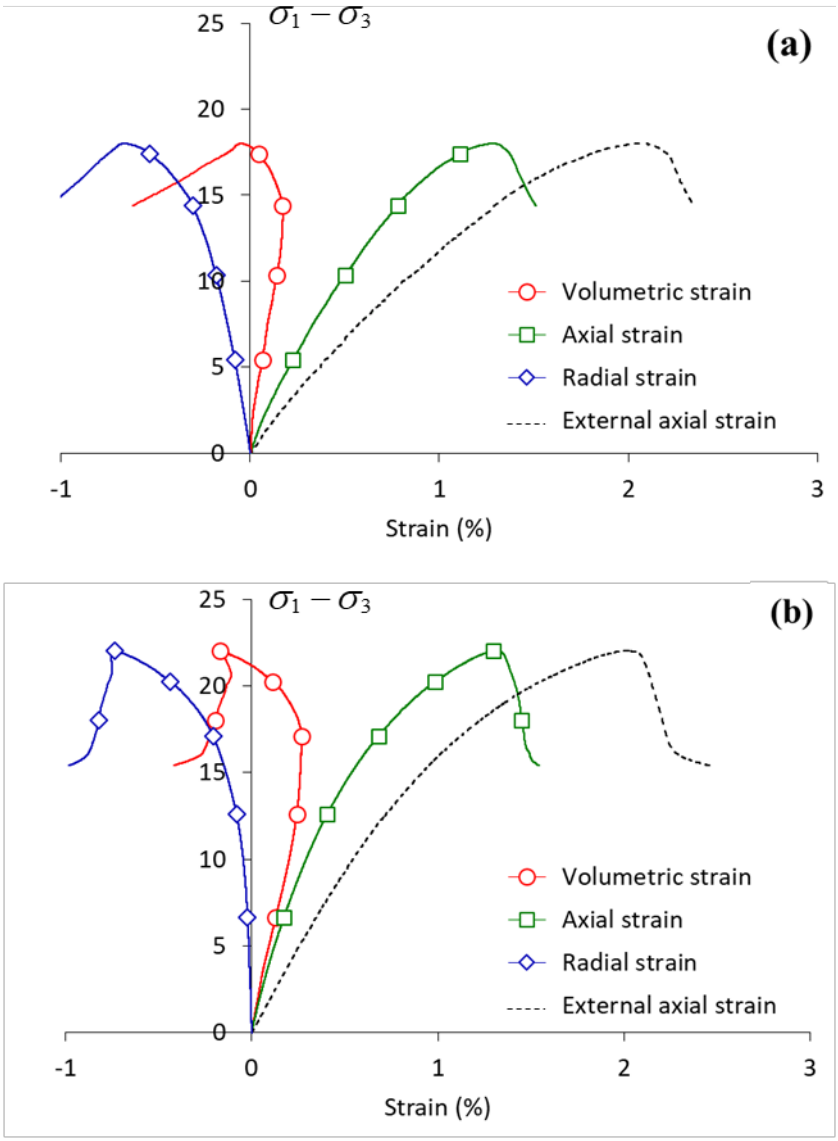


Figure 9. Stress strain curves of the drained sheared tests. External axial strains are in both cases larger than local ones. Similar contraction-dilation is observed in both cases, with a negative volumetric strain at peak (slight expansion) a) Specimen EST51338a under initial conditions close to in-situ mean effective stress (8 MPa); b) Specimen EST51338b under around 1.5 in-situ mean effective stress (12 MPa).

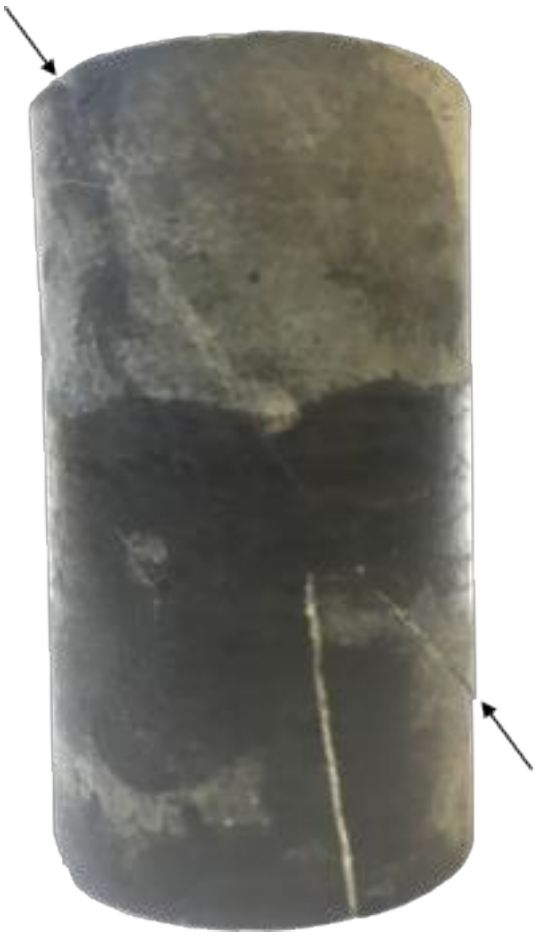

Figure 10. Sheared specimen (EST51338b), with shear plane inclined at an angle of 65° from horizontal.

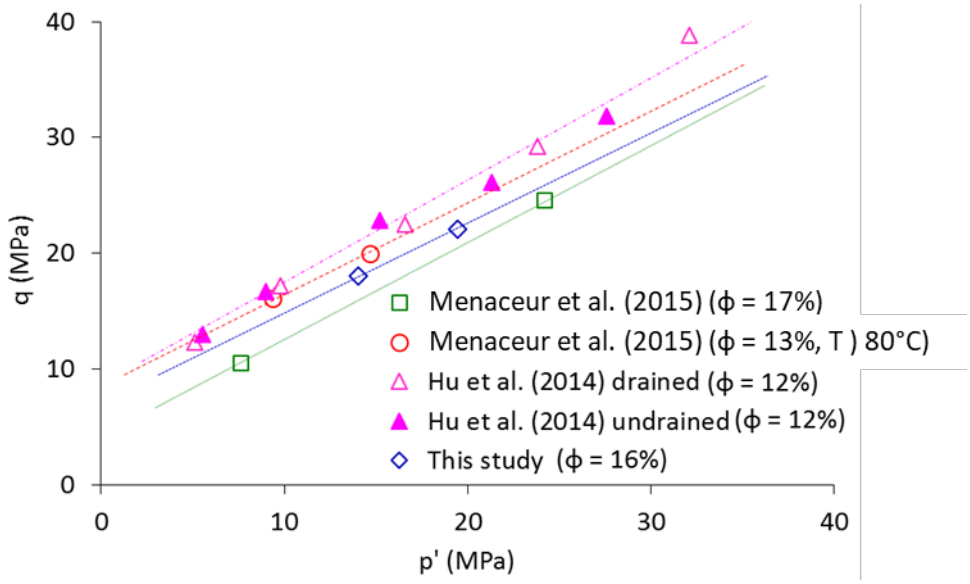


Figure 11. Comparison of the shear envelopes determined in this work (porosity 16%) with data of shear tests determined with different devices on saturated specimens of the Callovo-Oxfordian claystone with porosities between 12 and 17%: Menaceur et al. (2015) on hollow cylinder specimens; Hu et al. (2014) on small size triaxial specimens, either drained or undrained. Both devices had same drainage length (10 mm) with strain rates of $0.9\times10^{-7}$ $s^{-1}$ and $1.0\times10^{-7}$ $s^{-1}$, respectively. Shear envelopes are well organised with respect to the porosity.

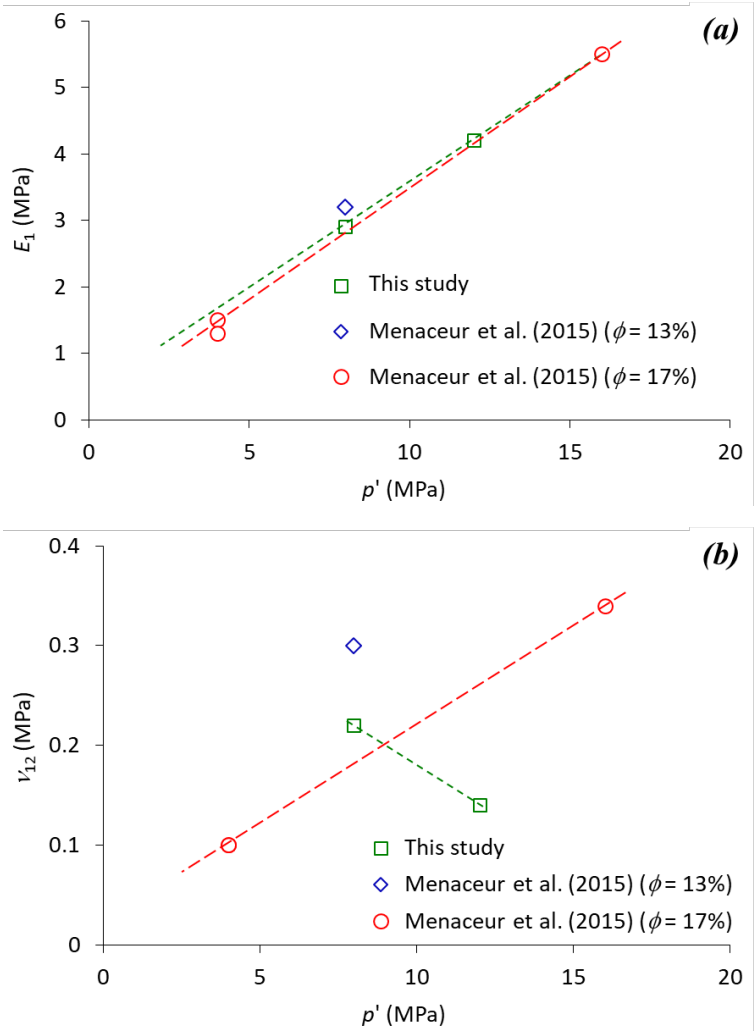


Figure 12. Comparison of the elastic parameters determined in this work with those of Menaceur et al. (2015): a) Young's modulus, with good comparability between tests and a linear increase with the confining stress; b) Poisson's ratio, with poor comparability, probably due to the difficulties in accurately measuring this parameter due to the very small radial strains mobilised.

Table 1. Initial characteristics of the tested specimens.

| ID Ech. | $w$ (%) | $\rho$ (Mg/m$^3$) | $\rho_d$ (Mg/m$^3$) | $e$ | $S_r$ (%) | $\phi$ (%) | Suction (MPa) |
|---|---|---|---|---|---|---|---|
| EST51338a | 5.97 | 2.41 | 2.27 | 0.19 | 87.9 | 16.2 | 36.2 |
| EST51338b | 5.97 | 2.41 | 2.27 | 0.19 | 87.9 | 16.2 | 36.2 |

Table 2. Strength and elastic parameters of the tested specimens of COx claystone.

| Test | $\sigma'$ (MPa) | $q_{max}$ (MPa) | $E_1$ (GPa) | $v_{12}$ (-) |
|---|---|---|---|---|
| EST51338a | 8 | 18 | 2.9 | 0.22 |
| EST51338b | 12 | 22 | 4.2 | 0.14 |